A Complex Gaussian Process Framework for Coherent ECGI Mapping and Isthmus Identification in Reentrant VT

Carlos Fambuena-Santos[1,2], María Correas[1], Andrea Cano[2], Jana Reventós[2], Jean B Guichard[3]
Andreu Porta[3], Ivo Roca-Luque[3], Alfred Peris[4], Andreu M Climent[1,2], María S Guillem[1,2]

[1] ITACA Institute, Universitat Politècnica de València, València, Spain
[2] CorifyCare SL, Madrid, Spain
[3] Arrhythmia Section, Institut Clínic Cardiovascular, Hospital Clínic, Barcelona, Spain
[4] Institut Universitari de Matemàtica Pura i Aplicada, Universitat Politècnica de València

Abstract

Standard non-invasive electrocardiographic imaging (ECGI) struggles with the spatial incoherence caused by circular activation in reentrant ventricular tachycardia (VT), hindering critical isthmus identification. This work introduces a novel spatiotemporal approach using Complex Gaussian Processes (CGP) to explicitly model the circular topology of local activation times (LATs), improving spatial consistency. The resulting high-resolution LAT maps are used to compute propagation velocity and curl, hypothesizing that the VT isthmus corresponds to regions of slow conduction and high curl. Evaluated on simulated and patient VT data, CGP-derived maps showed significantly better spatial coherence and more accurate propagation direction reconstruction compared to standard deflection-based methods (mean cosine angle 0.81 vs 64). Applying the velocity/curl criteria to CGP maps enabled more precise isthmus localization in simulations and showed concordance with clinical annotations in patients, presenting CGP as a promising non-invasive tool for improved VT circuit analysis.

1. Introduction

Catheter ablation targets the ventricular tachycardia (VT) isthmus, but invasive mapping is often precluded by hemodynamic instability. Electrocardiographic imaging (ECGI) reconstructs cardiac activation from body surface potentials, offering a panoramic view of the VT even in nonstable episodes. However, mapping reentrant VTs with ECGI is challenging due to its circular activation, that generates "cycle jumps". Standard ECGI methods relying on local deflections often yield spatially incoherent maps and fail to accurately represent the circuit across this discontinuity, hindering reliable isthmus localization.

Other spatiotemporal methods for LAT reconstruction in ECGI have been proposed with good results in sinus rhythm and pacing [1, 2]. However, these did not model the circular topology of reentry. We introduce a novel framework using Complex Gaussian Processes (CGP) to represent local activation times as complex phasors, inherently accommodating the circular nature of reentry and enforcing spatial consistency. Furthermore, we propose using these coherent CGP activation maps combined with an analysis of conduction velocity (CV) and curl, as a new strategy to non-invasively identify the critical VT isthmus. This combined CGP and propagation analysis approach is evaluated using simulated and patient VT data.

2. Materials and Methods

2.1. Data Acquisition and ECGI

Four reentrant VT simulations were generated using a human bi-ventricular mesh and an automata model with average edge length of 1.6 mm and 58529 nodes [3]. Reentry was induced via programmed stimulation, and isthmus locations were predefined geometrically. Body surface potentials (BSPs) were computed using a finite element torso model and corrupted with Gaussian noise (SNR = 20 dB).

Clinical data were obtained retrospectively from a patient undergoing VT ablation. BSPs were recorded using a 128-lead system (Corify Care S.L., Spain), and heart-torso geometries were reconstructed from pre-procedural MRI (ADAS 3D S.L. Spain). Electrode positions were co-registered to patient-specific anatomy. The study was approved by the hospital ethical committee and all patients gave informed consent.

BSP signals were bandpass (0.5–40 Hz) and notch (50 Hz) filtered, baseline corrected, and stable VT segments selected. Epicardial unipolar electrograms (EGMs) were reconstructed by solving the inverse problem using an infinite conductor formulation, the boundary element method

and the L2-norm Tikhonov regularization with the L-curve method for parameter tuning. Baseline LAT maps (dV/dt) were generated by identifying the time of minimum voltage deflection in each reconstructed EGM. These deflection-based maps served as the standard reference for evaluating the proposed method.

2.2. Complex Gaussian Process (CGP) Model

The VT cycle length (T_{CL}) was estimated from the BSPs. Point-wise LAT estimates (from dV/dt) were transformed into phase values and subsequently into complex phasors: $Z(x) = e^{i\phi(x)} = u(x) + i\,v(x)$.

Initial uncertainty estimates for each LAT value σ_{LAT} was derived from signal quality metrics [4]. A set of high confidence nodes x were identified based on these metrics and the LAT variance in these nodes $\sigma_{LAT(X)}$ was propagated to estimate the variance of the real ($\sigma_{u(X)}$) and imaginary ($\sigma_{v(X)}$) components in the complex representation. These variances formed the diagonal entries of the initial noise covariance matrix D_{aug} used in the CGP model.

We modeled the complex field Z across the epicardial mesh using a CGP framework. An augmented real-valued observation vector was constructed Y using real and imaginary parts. We employed a proper CGP model, defined by the augmented covariance matrix K:

$$\mathbf{Y} = \begin{bmatrix} u(x) \\ v(x) \end{bmatrix} \; ; \quad \mathbf{K} = \begin{bmatrix} K_{UU} & 0 \\ 0 & K_{VV} \end{bmatrix} \tag{1}$$

The auto-covariance matrices K_{UU} and K_{VV} belonging to the real and imaginary parts were modeled using Matérn kernels and all the hyperparameters were optimized by minimizing the negative log marginal likelihood as described in [4].

Finally, the CGP posterior mean and variance at each node x were calculated to define a circular Gaussian posterior distribution:

$$\begin{aligned} Z \mid Y \;\sim\; \mathcal{N}\Big(&\mu_Z + K_{ZY}K_{YY}^{-1}(Y - \mu_Y), \\ &K_{ZZ} - K_{ZY}K_{YY}^{-1}K_{YZ}\Big) \end{aligned} \tag{2}$$

Where Y constitutes the observation vector of high confidence LATs, Z the LATs in the whole ventricular geometry, K_{ZY} and K_{YZ} the cross-covariance matrices between the observation vector Y and the interpolated LATs.

2.3. LAT Map Analysis

We generated and compared four types of LAT maps. These included LATs derived directly from simulated electrograms (EGM LATs), LATs obtained by applying Laplacian spatial smoothing to the EGM LATs (Smoothed EGM LATs), LATs reconstructed via ECGI using a maximum slope (dV/dt) method and LATs reconstructed via ECGI using the CGP method.

To analyze activation dynamics, LATs from each map type were processed using consecutive time windows with a duration equal to the VT cycle length (T_{CL}) and 75% temporal overlap. The activation gradient ($\nabla\phi$) was calculated in the phase doamian for each window, scaled by $T_{CK}/2\pi$ to convert phase units to time, and then averaged across all windows to obtain a mean propagation vector field representative of the activation pattern. Conduction velocity (CV) and curl were subsequently computed from this mean vector field.

Finally, the reconstructed propagation vector fields derived from each of the four LAT mapping methods were compared against the simulation ground truth. Performance was evaluated by calculating the overall vector field Root Mean Square Error (RMSE) and the mean cosine of the vector angles to evaluate directional accuracy.

3. Results

Figure 1 introduces the simulation setup and provides a qualitative comparison of LAT map reconstruction accuracy. Panel A shows examples of simulated body surface. Panel B illustrates the different fibrosis distributions used across the four simulations, providing variability in the underlying substrate.

Panel C focuses on Simulation 2, comparing LAT maps obtained using different methods for the windows shown in panel A. The leftmost column shows the ground truth LATs derived directly from the simulated EGMs (EGM LATs), exhibiting sharp wavefronts across the VT channel. The second column shows the same ground truth LATs after applying spatial smoothing (Smoothed EGM LATs), replicating the spatial smoothing effect inherent to ECGI. In this map we can observe the propagation going through the scar and two vortices at each side of the channel. The third column displays the LAT maps reconstructed from ECGI using the standard deflection-based method (dV/dt), which appears less organized, struggling to capture the smooth progression seen in the ground truth. In contrast, the rightmost column shows the LAT maps obtained with our proposed coherent method (CGP LATs).

These maps demonstrate markedly improved spatial coherence and visually resemble the Smoothed EGM LATs much more closely in terms of wavefront shape and overall activation pattern in both windows, suggesting a more accurate representation of the underlying activation sequence.

Figure 2 illustrates results from a representative simulation. Panel A shows the ground truth propagation vector field derived directly from the simulated EGM LATs, while Panel B shows the field derived from a spatially smoothed

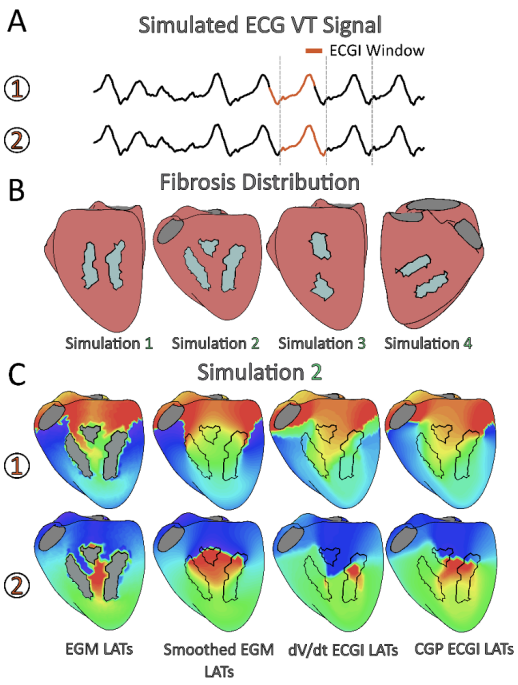

Figure 1. Simulation setup and LAT map comparison. (A) Example simulated VT BSPs. (B) Fibrosis distributions for the four simulations. (C) LAT map comparison (Simulation 2, 2 cycles): Ground Truth (EGM LATs), Smoothed EGM LATs, standard dV/dt ECGI, and proposed Coherent (CGP) ECGI. CGP LATs show improved coherence and better match to Smoothed GT than Deflection-Based LATs.

version of the ground truth LATs. This smoothing effect transforms the complex activation within the isthmus (black outlines) into a characteristic pattern consisting of a slow conduction (red/orange arrows in B) flanked by two vortices in the propagation which correspond to areas of high curl magnitude (in white). This smoothed pattern represents a realistic target in ECGI reconstruction.

In panels C and D the propagation fields reconstructed from ECGI data is shown using the standard deflection-based method (dV/dt) and our CGP method, respectively. Visually, the coherent propagation pattern (D) exhibits significantly better spatial organization and closer resemblance to the smoothed ground truth (B) compared to the standard deflection-based result (C). Quantitative analysis across all simulations (Panel E) confirms this observation. The coherent method achieved a lower overall vector field error (RMSE: 0.91 vs 1.08 ms/mm) and, critically, demonstrated substantially higher accuracy in reconstructing the propagation direction (Mean Cosine Angle: 0.81 vs 0.64) compared to the dV/dt method. The superior directional accuracy of the coherent method is key for correctly identifying the characteristic pattern.

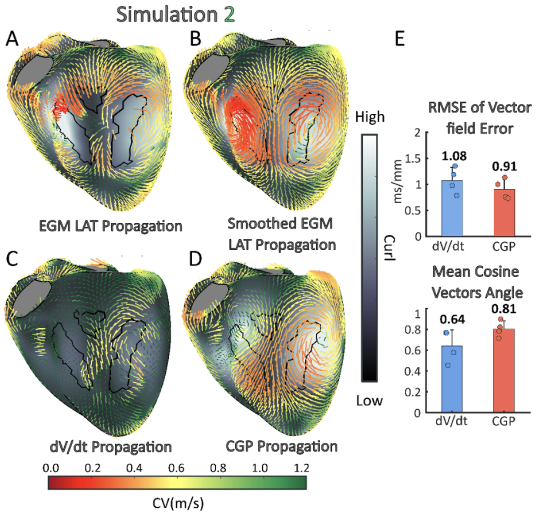

Figure 2. Coherent method improves ECGI propagation mapping in simulated VT. Propagation fields: (A) Ground Truth, (B) Smoothed GT, (C) dV/dt ECGI, (D) CGP ECGI. Arrow color: CV (0.0-1.2 m/s); outline: fibrosis distribution. CGP (D) visually matches smoothed GT (B) better than dV/dt (C). (E) Quantitatively (N=4), CGP has lower error (RMSE) mostly due to a better directional accuracy (Cosine Angle) than dV/dt.

In figure 3 the results from a representative patient are presented. Panel B compares LAT map sequences obtained via dV/dt (top) and our CGP approach (bottom). The CGP maps demonstrate significantly improved spatial coherence and smoother wavefront propagation compared to the standard method.

Consequently, derived propagation characteristics are enhanced. In panel C the conduction velocity and curl magnitude fields derived from dV/dt and CGP maps are compared in this patient. The CGP-derived fields are markedly smoother and more organized than the one obtained with the dV/dt method. In this way, our proposed pattern of slow conduction (red/orange arrows) and rotational activity (white regions) is clearer revealed in the CGP map and colocalizes nicely with the VT-channel area identified by the electrophysiologist (black outline). Additionally, in panel D the VT circuit identified using EAM is shown demonstrating perfect correspondence with the propagation obtained with our CGP method.

4. Discussion and Conclusions

This study presents a novel framework for non-invasive mapping of reentrant ventricular tachycardia (VT) from ECGI data, combining Complex Gaussian Processes (CGP) for LAT estimation with curl and velocity analy-

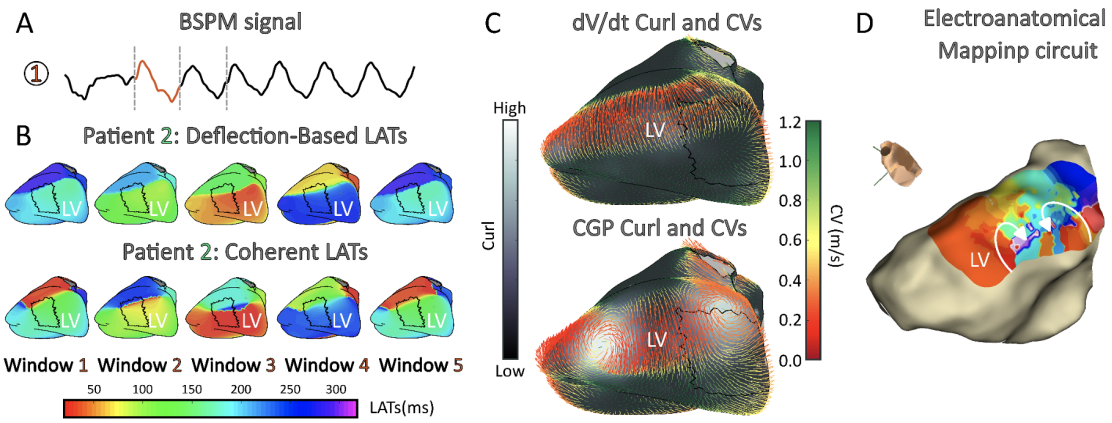

Figure 3. Comparison of deflection-based (dV/dt) and coherent LATs (CGP) obtained with ECGI in a patient. (A) Example of a BSP VT cycle. (B) LAT map sequences (dV/dt top, Coherent method bottom) for a patient, showing improved spatial coherence with the CGP method. (C) Conduction velocity (CV) and curl analysis derived from dV/dt maps (top) versus CGP maps for the same patient. CGP-derived analysis yields smoother CV fields and clearer curl patterns. (E) Electroanatomic map of the TV corroborating the circuit. LV: Left Ventricle; black outlines indicate regions containing the main ventricular tachycardia channel labelled by an electrophysiologist.

sis for isthmus identification. By modeling LATs as complex phasors, CGP captures the circular topology of reentrant activation, improving spatial coherence compared to standard deflection-based methods. The resulting LAT maps exhibit smoother and more physiologically consistent propagation patterns in both simulations and patient data.

Limitations include the small number of cases. Additionally, like many ECGI approaches, our current implementation focuses on epicardial reconstruction. Future work should involve validation in larger cohorts with detailed invasive mapping and explore extensions to incorporate transmural information.

In conclusion, the CGP-based framework enhances noninvasive ECGI of reentrant VT by addressing phase discontinuities and enabling novel isthmus localization criteria based on wavefront dynamics. This approach may support more accurate identification of ablation targets, potentially improving outcomes in VT treatment.

Acknowledgments

This work was supported by Agencia Estatal de Investigación: PID2023-149812OB-I00, CPP2021-008562. By ESF Investing in your future (RYC2018-024346-I) and by FEDER, EU (CPP2023-01050).

References

[1] Duchateau J, Potse M, Dubois R. Spatially coherent activation maps for electrocardiographic imaging. IEEE Transactions on Biomedical Engineering 2017;64(5):1149–1156.

[2] Cluitmans M, et al. Spatiotemporal approximation of cardiac activation and recovery isochrones. Journal of Electrocardiology 2022;71:1–9.

[3] Herrero-Martin C, Fambuena-Santos C, Guillem MS, Climent AM, Hernandez-Romero I. Tailoring process for the regional personalization of atrial fibrillation with a novel cardiac model. In Computing in Cardiology (CinC), volume 2022-Septe. 2022; 2022–2025.

[4] Coveney S, et al. Gaussian process manifold interpolation for probabilistic atrial activation maps and uncertain conduction velocity: Gaussian process manifold interpolation. Philosophical Transactions of the Royal Society A Mathematical Physical and Engineering Sciences 2020;378(2173).

Address for correspondence:

Carlos Fambuena Santos
ITACA. Edificio 8G acceso B. Universitat Politècnica de València. Camino de Vera s/n. 46022 Valencia, Spain.
carfamsa@upvnet.upv.es